Revealing Excited State Interactions by Quantum-Chemical Modeling of Vibronic Activities: The R2PI Spectrum of Adenine†

Irene Conti,‡ Eugenio Di Donato,‡,§ Fabrizia Negri,*,‡,§ and Giorgio Orlandi*,‡,§

Dipartimento di Chimica "G. Ciamician", Universitá di Bologna, Via F. Selmi, 2, 40126 Bologna, Italy, and INSTM, UdR Bologna, Italy

Received: June 19, 2009; Revised Manuscript Received: July 31, 2009

We present a computational study encompassing quantum-chemical calculations of the ground and low-lying excited states of 9*H*-adenine and modeling of vibronic activities associated with the $S_0 \rightarrow L_b$ and $S_0 \rightarrow n\pi^*$ transitions. Minima on the ground and excited states and the saddle point on the $n\pi^*$ potential energy surface are determined with CASSCF calculations. Vibrational frequencies are computed at the same level of theory on ground and excited states while transition dipole moments and oscillator strengths are estimated, at the optimized geometries, with CASPT2//CASSCF calculations. Modeling of vibronic activities includes both Franck−Condon and Herzberg−Teller induced contributions. While the adopted harmonic approximation is acceptable for the $S_0 \rightarrow L_b$ transition and allows the assignment of several observed bands in the R2PI spectrum of adenine, the computed anharmonic potential along the puckering coordinate in the $n\pi^*$ state requires a different treatment. To this end the vibronic levels and intensities associated with vibronic transitions in the puckering coordinate are evaluated by numerical solution of the 2D potential including the anharmonic puckering coordinate. All the remaining vibrational coordinates are treated as harmonic. On the basis of the modeling, the four major bands in the R2PI spectrum of adenine are assigned, along with a number of minor bands in the spectra.

1. Introduction

The DNA bases show a remarkable degree of photostability that is essential for the preservation of the genetic information. The photophysical properties of these compounds have been discussed in several contributions,[1,2] while the ultrafast dynamics of their excited states were reviewed recently by Kohler and co-workers.[3] In this paper we consider the lowest electronic excited states of the 9*H* isomer of adenine (Ade), which is shown in Scheme 1.

In its ground state (S_0) Ade is roughly planar, except for the pyramidalization of the NH_2 group.[1] In vapor, its absorption spectrum shows two intense bands with maxima[3] at 250 and 207 nm, assigned to the L_a and B_b excited states of $\pi\pi^*$ nature, respectively. In solution the absorption bands of the two states are slightly red-shifted.[4]

In the gas phase, the lowest excited singlet states are a $n\pi^*$ state, the L_b and the L_a $\pi\pi^*$ states.[3] For its large transition moment to S_0, the L_a state is responsible for most of the absorption observed in the spectral region below 5 eV.

Molecular beam spectra of Ade obtained by resonance enhanced two-photon ionization (R2PI) and by laser induced fluorescence (LIF) showed a number of resolved vibronic bands in the region 35 500 to about 36 700 cm^{-1}, followed by a broad continuous absorption in the range from 36 700 to 40 000 cm^{-1}, where the recorded spectrum ends.[5−11] Beside the weak and lowest energy band at 35 497 cm^{-1}, called band A, the three bands C, D, and E observed at 36 062, 36 105, and 36 248 cm^{-1}, respectively, were investigated in detail. The very weak band B was shown to belong to the 7H isomer of Ade. Bands A and D were interpreted as the origins of the $n\pi^*$ (S_1) and ^1L_b (S_2) states, respectively.[6] These assignments were subsequently confirmed and extended by the groups of de Vries and Kleinermanns.[8,11] The spectral patterns observed upon mono-deuteration showed that bands C and E belong to the same electronic state, while the D band appears to belong to a different state.[9] Furthermore, the vibrational structure of the fluorescence obtained by exciting bands C and D is different.[10] These observations supported strongly the assignment of bands C and E to the $^1n\pi^*$ state and of band D to the origin of the L_b state. Interestingly, no vibronic band in this region was assigned to the L_a state.

SCHEME 1: Adenine Structure with Atom Numbering

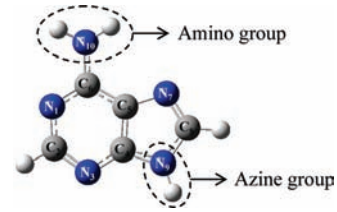

In gas phase the measured lifetime[7] of Ade excited to the D band is ≈9 ps and it was estimated to be even longer, about 40−50 ps, on the basis of the Lorentzian linewidths associated with the rovibronic transitions.[12]

The rotational profiles of the C, D, and E bands, measured in a recent study,[13] allowed to estimate more accurately the lifetimes of the relevant vibronic states and to determine the Cartesian components, along the inertial axes, of the associated absorption transition moments.[13] This in turn provides precious information on the dominant vibronic interactions perturbing the $n\pi^*$ and L_b states. The E band was found to have the same

† Part of the "Vincenzo Aquilanti Festschrift".

* Corresponding authors. E-mail: G.O., giorgio.orlandi@unibo.it; F.N., fabrizia.negri@unibo.it.

‡ Universitá di Bologna.

§ INSTM.

10.1021/jp905795n
Published on Web 09/15/2009

rotational contour as the D band, and both were shown to derive their intensities from a predominantly in-plane polarized transition.[13] On the contrary, the C band was shown to have a different rotational contour indicating a transition polarized mainly perpendicular to the molecular plane.[13]

The purpose of this paper is to supplement the above spectroscopic observations with quantum chemical calculations, followed by modeling of the relevant vibronic structures, to provide a more detailed interpretation of the observed bands. To this end we employed CASSCF and CASPT2 levels of theory to predict electronic energy gaps and transition moments at the equilibrium geometries of the S_0, $n\pi^*$, and L_b states. Vibrational normal coordinates and frequencies were computed in each electronic state and Franck−Condon (FC) and Herzberg−Teller (HT) activities for the relevant modes were modeled to provide elements for the interpretation of the Ade vibronic spectrum. A special attention and treatment was reserved to the ring puckering mode, which is characterized by an anharmonic double minimum potential in the $n\pi^*$ state. To the best of our knowledge only one computational study[14] concerning the spectroscopy of excited states of Ade was reported so far, but it did not address the specific questions considered here.

2. Computational Details

2.1. Quantum Chemical Calculations. The S_0, $n\pi^*$, and L_b stationary points were computed at the ab initio level in the framework of the CASSCF strategy.[15,16] The chosen active space included 7 π orbitals (4 bonding and 3 antibonding) plus two doubly occupied nitrogen lone pairs, resulting in an active space of 9 orbitals and 12 electrons. The standard 6-31+G** basis set was used.

Geometry optimizations were fully unconstrained, with the exception of the in-plane $n\pi^*$ saddle point, which was obtained by imposing the planarity constraint on the purinic skeleton. To avoid root-flipping problems, state average calculations including the ground state beside the selected excited state (with equal weights) were employed to optimize excited state geometries. CASSCF calculations were followed by single point CASPT2[16] computations on the optimized relevant structures to account for dynamical correlation energy. Vibrational frequencies and normal modes were computed at CASSCF level using the same orbital space employed for structure optimization. A step-size of 0.001 Å for the excited states and of 0.005 Å (the default value, since ground state vibrational frequencies are less affected by numerical instabilities) for the ground state were employed for numerical differentiation.

Electronic excitation energies and transition moments, at all the relevant atomic structures, were computed with a state average CASSCF procedure including, with equal weights, the first 8 singlet states. The molecular orbitals, energies and reference functions were used in subsequent CASPT2 calculations. An "imaginary shift"[17] of 0.25 au was employed for all state averaged CASPT2 computations to eliminate possible intruder states.

The CASSCF State Interaction (CASSI)[15] method was used to calculate the transition dipole moments (TDM). Oscillator strengths were evaluated by using CASSCF transition moments and CASPT2 energy gaps. All computations were performed with the tools available in the Gaussian 03[18] and MOLCAS-6.2[19] quantum-chemistry programs.

2.2. FC and HT Contributions to Vibronic Activities of Harmonic Modes. Within the Born−Oppenheimer approximation, the TDM between vibronic states, that is, vibrational states p and m belonging to two electronic states K and J, is

$$M_{Kp,Jm} = \langle K,p|\mu|J,m\rangle = \langle p|\mu_{K,J}|m\rangle \quad (1)$$

where $\mu_{K,J}$ is the electronic TDM and p and m are multidimensional vibrational wave functions. According to the HT mechanism we can expand the TDM as a Taylor series in the nuclear coordinates about the equilibrium nuclear configuration

$$M_{Kp,Jm} = \mu^{o}_{K,J}\langle p|m\rangle + \sum_i \left(\frac{\partial \mu_{K,J}}{\partial Q_i}\right)\langle p|Q_i|m\rangle + \ldots \quad (2)$$

Each $(\partial\mu_{K,J}/\partial Q_i)$ first derivative with respect to the ith normal mode may contribute to the HT induced false origin's intensities in the spectra.[20] Assuming the harmonic approximation, negligible Duschinsky effect, and identical frequencies in the K and J electronic states, the intensity of each false origin ($0 \rightarrow 1$ for the ith mode) in the spectrum, when all other vibrational wave functions are in their m_j level of the final electronic state, is given by[20,21]

$$I_{K0_i,J1_i} \propto M_{K0_i,J1_i}{}^2 \prod_{j\neq i}\langle 0_j|m_j\rangle^2 = \left[\left(\frac{\partial \mu_{K,J}}{\partial Q_i}\right)\sqrt{\frac{\hbar}{2m\omega_i}}\right]^2 \prod_{j\neq i}\langle 0_j|m_j\rangle^2 \quad (3)$$

where it has been assumed that, in dimensionless coordinates q_i, $\langle 0_i|q_i|1_i\rangle = (1/2)^{1/2}\langle 1_i|1_i\rangle$.

The derivatives in eq 3 were evaluated numerically using the CASSCF theory and considering a state average over the first 8 states. Excited state normal coordinates and frequencies were employed to estimate induced intensities. For each computed TDM the associated oscillator strength contribution can be obtained as

$$f_i = \frac{2}{3} h\nu_{K0_i,J1_i} M_{K0_i,J1_i}{}^2 \prod_{j\neq i}\langle 0_j|m_j\rangle^2 \quad (4)$$

where $h\nu_{K0_i,J1_i}$ is the energy difference, in Hartree, between the selected vibronic states of the $K \leftrightarrow J$ electronic transition, taken from the experimental data (see below) and M is in e bohr.

Equation 2 underscores that, for low-symmetry molecules such as Ade, and for weakly allowed electronic transitions, each vibration can contribute intensity both through the HT and the FC mechanisms[22,23] The FC structure[24−28] associated with the absorption spectrum was evaluated along the lines described in previous work.[29] Assuming the harmonic approximation, negligible Duschinsky effect and identical frequencies in the K and J states, the displacement parameter B_i relative to the $K \rightarrow J$ transition and the ith mode is

$$B_i = \sqrt{\frac{\omega_i}{\hbar}}\{X_K - X_J\}\mathbf{M}^{1/2}\mathbf{L}_i(K) \quad (5)$$

where $\mathbf{X}_K$ is the $3N$ dimensional vector of the equilibrium Cartesian coordinates of the Kth state (here S_0 or S_1), $\mathbf{M}$ is the $3N \times 3N$ diagonal matrix of the atomic masses, and $\mathbf{L}_i(K)$ is the $3N$ vector describing the normal coordinate Q_i of the K state in terms of mass-weighted Cartesian coordinates. CASSCF optimized geometries, vibrational frequencies, and normal coordinates were employed. In the harmonic approximation and

assuming identical frequencies in the two electronic states, the FC intensity of a band corresponding to the $n = [n_1, n_2, n_3, ..., n_N]$ vibrational quantum is given by

$$I_{K0,Jn} \propto \prod_j \langle 0_j|n_j\rangle^2 = \prod_j e^{-\gamma_j}\frac{(\gamma_j)^{n_j}}{n_j!} \quad (6)$$

where $\gamma_i = {}^1/_2(B_i)^2$. Notice that

$$\frac{I^i_{K0,J1}}{I_{K0,J0}} = \frac{I^i_{0-1}}{I_{0-0}} = \gamma_i \quad (7)$$

$$I_{K0,J0} = I_{0-0} \propto \prod_j \langle 0_j|0_j\rangle^2 = \prod_j e^{-\gamma_j} = e^{-\gamma_{tot}} \quad (8)$$

with $\gamma_{tot} = \sum_j \gamma_j$.

To account for possible Duschinsky[30] normal mode mixing, vibrations of the excited state were considered in the simulation of the absorption spectra.[31] While this approach is approximate, and less rigorous than that discussed in recent works,[22−28,32,33] it is justified when minor Duschinsky rotation[30] upon excitation is computed for the active frequencies.

2.3. Vibronic Activities of Anharmonic Modes. The $S_0 \leftrightarrow S_1(n\pi^*)$ vibronic activities for the puckering coordinate, which is characterized by an anharmonic double-minimum S_1 potential, were evaluated by solving the vibrational wave functions numerically using the flexible 2D model of Meyer.[34] The model is based on a two-dimensional potential describing both the ground and the excited states. The first coordinate was defined simply by the puckering angle ϕ, that is, the improper dihedral angle $\phi(C_2N_1N_3C_5)$, keeping all the other structure parameters fixed. Following previous work,[35,36] the S_1 potential was expressed as the sum of a quadratic and a quartic term.

In the flexible model we included a second mode, the C_2-H out-of-plane bending, labeled α, which is naturally coupled to the C_2 puckering as indicated by the optimized structure of the $n\pi^*$ state. On the basis of computed vibrational frequencies and coordinates for the $n\pi^*$ state, the α coordinate was assigned the frequency of ca. 478 cm^{-1}. Following previous work,[35,36] we introduced a coupling term $V(\phi,\alpha) = e\phi\alpha$, where $e = 0.7$ cm^{-1} $grad^{-2}$.

The two-dimensional $n\pi^*$ potential in the α, ϕ space, reads

$$V_{n\pi^*}(\phi,\alpha) = a\phi^2 + b\phi^4 + c\alpha^2 + d\alpha^4 + e\phi\alpha \quad (9)$$

where the coefficients a ($a < 0$) and b were determined by using, as a starting guide, the CASSCF computed dihedral angle $\phi_0 = 36°$ associated with the $n\pi^*$ minimum (see below), and the computed energy barrier between the $n\pi^*$ saddle point and the out of plane distorted $n\pi^*$ minimum (see section 3). Along both coordinates we selected a number (25) of uniformly spaced ϕ_i (α_j) values for integration within the interval of $+75° < \phi < -75°$ with respect to the planar geometry.

In the ground state, on the basis of our computed frequencies and coordinates (see the Supporting Information) and on previous work,[37] the puckering and the C_2-H bending modes were considered harmonic with frequencies of 558 and 975 cm^{-1}, respectively, and the $V(\phi,\alpha)$ coupling term was neglected.

Since the model is considerably simplified, several combinations of the two-dimensional potential parameters, starting from those quantum chemically computed, were explored to tune the computed vibrational eigenvalues and observables in better agreement with the experimental results. The potential energy parameters are collected in Table S1 (Supporting Information).

To evaluate the vibronic structure of the $S_0 \rightarrow n\pi^*$ transition, we need the expression for geometry dependence of $S_0 \rightarrow n\pi^*$ TDMs. The CASSCF computed TDM components $\mu^x_{S_0,n\pi^*}(\phi,\alpha)$, $\mu^y_{S_0,n\pi^*}(\phi,\alpha)$ and $\mu^z_{S_0,n\pi^*}(\phi,\alpha)$ were found to depend substantially on the ϕ puckering and very weakly on the α coordinate. They are well represented by the following expressions

$$\begin{aligned}\mu^x_{S_0,n\pi^*} &= a_x\phi/(1 + b_x\phi^2)\\ \mu^y_{S_0,n\pi^*} &= a_y\phi/(1 + b_y\phi^2)\\ \mu^z_{S_0,n\pi^*} &= a_z/(1 + b_z\phi^2)\end{aligned} \quad (10)$$

where the a and b coefficients are collected in Table S2 while the fitted potential and TDMs are depicted in Figure S1 (see the Supporting Information). The above expressions underscore the negligible dependence on the α coordinate of the three transition moments: $\mu^w_{S_0,n\pi^*}(\phi,\alpha) = \mu^w_{S_0,n\pi^*}(\phi)$, with $w = x, y, z$.

Employing the computed numerical pth and mth vibrational eigenfunctions for the ground and excited electronic states, $\chi^{S_0}_p(\phi_i,\alpha_j)$, $\chi^{n\pi^*}_m(\phi_i,\alpha_j)$, and the above-defined TDMs, the overlap integrals and the vibronic transition moments can be readily determined by numerical integration over the 25 selected points along each of the two coordinates

$$\begin{aligned}S_{S_0p,n\pi^*m} &= \langle\chi^{S_0}_p|\chi^{n\pi^*}_m\rangle = \sum_{i,j}^{25}\chi^{S_0}_p(\phi_i,\alpha_j)\,\chi^{n\pi^*}_m(\phi_i,\alpha_j)\\ M^w_{S_0p,n\pi^*m} &= \langle\chi^{S_0}_p|\mu^w_{S_0,n\pi^*}|\chi^{n\pi^*}_m\rangle =\\ &\quad \sum_{i,j}^{25}\chi^{S_0}_p(\phi_i,\alpha_j)\,\mu^w_{S_0,n\pi^*}(\phi_i,\alpha_j)\,\chi^{n\pi^*}_m(\phi_i,\alpha_j)\end{aligned} \quad (11)$$

where $w = x, y, z$ represents a Cartesian component. The vibrational eigenvalues and eigenvectors for both ground and excited states along with vibrational overlaps and vibronic transition moments are usually well predicted with this procedure.[35,36]

3. Results and Discussion

3.1. Excited State Energies and TDMs. ***3.1.1. Ground State Structure and Vertical Excitation Energies.*** The CASSCF(12,9)/6-31+G** optimized ground state structure, labeled $(S_0)_{min}$, is almost planar with a slightly pyramidalized amino group (the π orbital axis vector (POAV) angle θ is 93.43°). Similar structures are obtained with the (14,11) and (12,10) active spaces (see Figure S2 in the Supporting Information section) in striking agreement with the recent results obtained by the vibrational transition moment angles method.[38] Since the barrier's height for the amino group inversion of Ade is found to be only 0.01 eV,[38] the two amino hydrogens are not confined in one of the two minima but oscillate on the whole anharmonic potential. This is confirmed by the small inertial defect (−0.2) found in microwave (MW) spectra.[39] The other structural parameters, which are shown in Figure 1, are in agreement with previous experimental[40] and theoretical results.[41−44]

In Table 1 we report the CASSCF and the CASPT2 energies of the most relevant excited states (L_a, L_b, $n\pi^*$, and B_b)

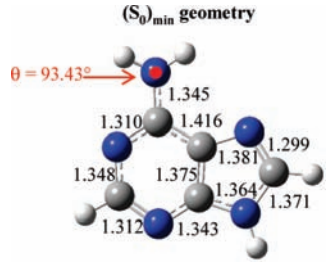

Figure 1. CASSCF(12,9)/6-31+G** optimized bond lengths (Å) of Ade in $(S_0)_{min}$. The value of the POAV angle θ for the amino group is also indicated.

computed at the S_0 equilibrium geometry, usually referred to as the "vertical" excitation energies and the corresponding $S_0 \rightarrow S_i$ oscillator strengths. As reported in previous studies,[41,43,45] the CASPT2 energies of the three lowest excited states, $^1n\pi^*$, ^1L_a, and ^1L_b, are similar. The $^1n\pi^*$ state has the lowest energy (5.09 eV), and the ^1L_b and the ^1L_a energies are higher by 0.04 and 0.15 eV, respectively. The oscillator strengths of the $S_0 \rightarrow {}^1n\pi^*$, $S_0 \rightarrow {}^1L_b$, and $S_0 \rightarrow {}^1L_a$ transitions are $\approx 10^{-2}$, $<10^{-3}$, and 0.22, respectively, and thus the low-energy absorption of Ade is dominated by the $S_0 \rightarrow {}^1L_a$ transition. At higher energy the most important state is the ^1B_b state computed at 6.26 eV with the largest oscillator strength (0.48).

The computed vertical transitions energies and oscillator strengths shown in Table 1 correlate qualitatively well with the experimental absorption spectrum. They are also in line with the results of calculations by Merchan,[42] Perun,[46] and Chen,[47] although they appear to be very dependent on the details of calculation. A critical observable is apparently the oscillator strength of the $S_0 \rightarrow {}^1L_a$ transition for which values ranging from 0.14[46] and 0.33[47] were reported.

3.1.2. Excited State Optimized Structures and Energies. The CASSCF(12,9)/6-31+G** optimized structures of the lowest excited states, $(^1L_b)_{min}$, $(^1n\pi^*)_{min}$, and $(^1n\pi^*)_{saddle}$, are somewhat different from S_0, as shown in Figure 2a $(^1L_b)_{min}$ and Figure 2b,c $(^1n\pi^*)$. The structure optimization in the ^1L_b state leaves the molecule almost planar and decreases the ^1L_b energy by about 0.41 eV with respect with the vertical excitation energy. At the same time the NH_2 pyramidalization increases to a POAV angle θ of 101.48°.

The structure of the $(^1n\pi^*)_{min}$ (Figure 2b) is nonplanar because of the out-of-plane displacement of the C_2 carbon atom (the puckering distortion of the hexagonal ring), which is defined by the improper dihedral angle $\phi(C_2N_1N_3C_5)$ whose equilibrium value is computed to be 36°.

In addition, the POAV angle θ of the C_2 center is computed to be 104.11°, while that of the NH_2 group is 98.65°. The computed equilibrium structure is very similar to that reported in recent studies.[43] The CASSCF/CASPT2 (state average over 8 states) energy of the twin minima is 4.21 eV, that is, 0.88 eV lower than the vertical excitation energy, and 0.63 eV below the $n\pi^*$ optimized structure under the constraint of planarity for the purinic skeleton $(^1n\pi^*)_{saddle}$, which is a saddle in the $n\pi^*$ PES and shows a pyramidalization (POAV angle θ) of the NH_2 group of 99.71°. By comparison, the $n\pi^*$ stabilization energy with respect to vertical excitation was found, in previous studies, to be 1.027,[46] 0.449,[47] and 0.47 eV.[44] This indicates that the stabilization of the $n\pi^*$ state is sensitive to the details of the calculations.

The computed excited state energies and transition moments depend to some extent on the approximations chosen, like the atomic basis set and the active space size. More important for the modeling of vibronic activities discussed in this work is the observation that, for a given basis set and CAS space, the

TABLE 1: CASSCF(12,9)/6-31+G and CASPT2//CASSCF (Italic) Relative Energies[a] (in eV) and Oscillator Strengths (f) Computed at the $(S_0)_{min}$, $(^1L_b)_{min}$, $(^1n\pi^*)_{saddle}$, and $(^1n\pi^*)_{min}$ Structures**

	$(S_0)_{min}$		$(^1L_b)_{min}$		$(^1n\pi^*)_{saddle}$		$(^1n\pi^*)_{min}$	
	E (eV)	f	E (eV)	f	E (eV)	f	E (eV)	f
S_0	0.00		0.22		0.93		1.56	
	0.00		*0.09*		*0.81*		*1.40*	
$n\pi^*$	6.07	1.1×10^{-2}	6.01	1.0×10^{-2}	5.74	4.4×10^{-3}	5.17	5.2×10^{-3}
	5.09	*9.4×10^{-3}*	*4.98*	*8.7×10^{-3}*	*4.84*	*3.7×10^{-3}*	*4.21*	*4.0×10^{-3}*
L_b	5.61	3.5×10^{-4}	5.19	2.0×10^{-3}	6.11	2.6×10^{-3}	6.22	6.2×10^{-3}
	5.13	*3.2×10^{-4}*	*4.72*	*1.9×10^{-3}*	*5.55*	*2.4×10^{-3}*	*5.60*	*5.3×10^{-3}*
L_a	7.03	0.29	6.97	0.24	7.18	0.24	7.34	0.11
	5.24	*0.22*	*5.07*	*0.18*	*5.46*	*0.19*	*5.75*	*0.08*
B_b	8.21	0.63	7.91	0.39	8.66	0.28	9.18	0.48
	6.26	*0.48*	*6.05*	*0.30*	*7.28*	*0.24*	*7.21*	*0.36*

[a] A state averaging procedure over eight states with equal weights was adopted.

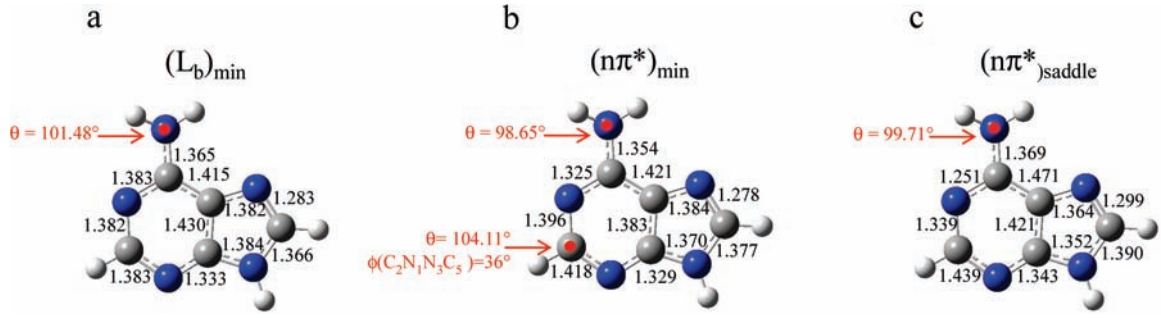

Figure 2. CASSCF(12,9)/6-31+G** bond lengths (Å) of Ade for the optimized structures of (a) $(^1L_b)_{min}$, (b) $(^1n\pi^*)_{min}$, and (c) $(^1 n\pi^*)_{saddle}$. The values of the POAV angle θ for the amino group and the C_2 pyramidalization along with the improper dihedral angle ϕ describing the puckering are indicated.

TABLE 2: CASSCF(12,9)/6-31+G Relative Energies (in eV) Computed at the $(S_0)_{min}$, $(^1L_b)_{min}$, $(^1n\pi^*)_{saddle}$, and $(^1n\pi^*)_{min}$ Structures[a]**

	$(S_0)_{min}$	$(^1L_b)_{min}$	$(^1n\pi^*)_{saddle}$	$(^1n\pi^*)_{min}$
S_0	0.0	0.44	1.10	1.80
$n\pi^*$			5.71	5.35
L_b		5.51		

[a] A state averaging procedure over two states with equal weights was adopted, except for the energy at the $(S_0)_{min}$ structure.

state averaging procedure influences considerably the detailed energetics of the $n\pi^*$ anharmonic potential. In Table 2 we collected the $S_0 \leftrightarrow n\pi^*$, and $S_0 \leftrightarrow L_b$ excitation energies computed at the relevant optimized structures at CASSCF level by averaging over only two states, as described in section 2.1. While the CASSCF excitation energies have somewhat changed, the trend is confirmed. However, the profile of the anharmonic potential of the $n\pi^*$ state emerging from the two sets of state averaging procedures (Tables 1 and 2) is rather different. In one case (state average over 8 states) the computed CASSCF barrier's height is 0.57 eV (ca. 4600 cm^{-1}) while in the other case (state average over only 2 states) the barrier's height drops to 0.37 eV (ca. less than 3000 cm^{-1}). Considering the CASPT2 correction, in the first case the barrier increases slightly to 0.63 eV (ca. 5100 cm^{-1}). The wide range of computed E_b values indicates that the modeling of this out of plane deformation is very sensitive to the wave function definition. In the light of the above computed results and considering the approximations in the definition of the anharmonic potential, we expect that refinement of the potential parameters (see section 2.3) will be required to get the best agreement with the experimental results.

The oscillator strengths for the $S_0 \rightarrow S_i$ transitions computed at the $(^1L_b)_{min}$, $(^1n\pi^*)_{min}$, and $(^1 n\pi^*)_{saddle}$ optimized geometries are somewhat different than those at the $(S_0)_{min}$ structure. In particular, not only the magnitude but also the Cartesian components (see also Table S5, Supporting Information), that is, the orientation of the transition moments, appear to change. This is shown in Figure 3, where the CASSCF computed magnitudes and directions of the transition moments are collected for the relevant optimized structures.

The largest differences in TDMs are found for the $S_0 \leftrightarrow n\pi^*$ transition computed at the $(^1n\pi^*)_{min}$ and at the $(^1n\pi^*)_{saddle}$ structures. The sizable in-plane components of the $S_0 \leftrightarrow n\pi^*$ TDM at the $(n\pi^*)_{min}$ suggest that a mixing between $\pi\pi^*$ and $n\pi^*$ states has occurred.[44] This implies that the vibronic structure of the $n\pi^*$ excitation spectrum cannot be satisfactorily described by the usual first order FC and HT procedures (see section 2.2), at least as far as the puckering coordinate contribution is involved. Furthermore, the anharmonic (double-minimum) character of the puckering potential, requires a specific treatment.

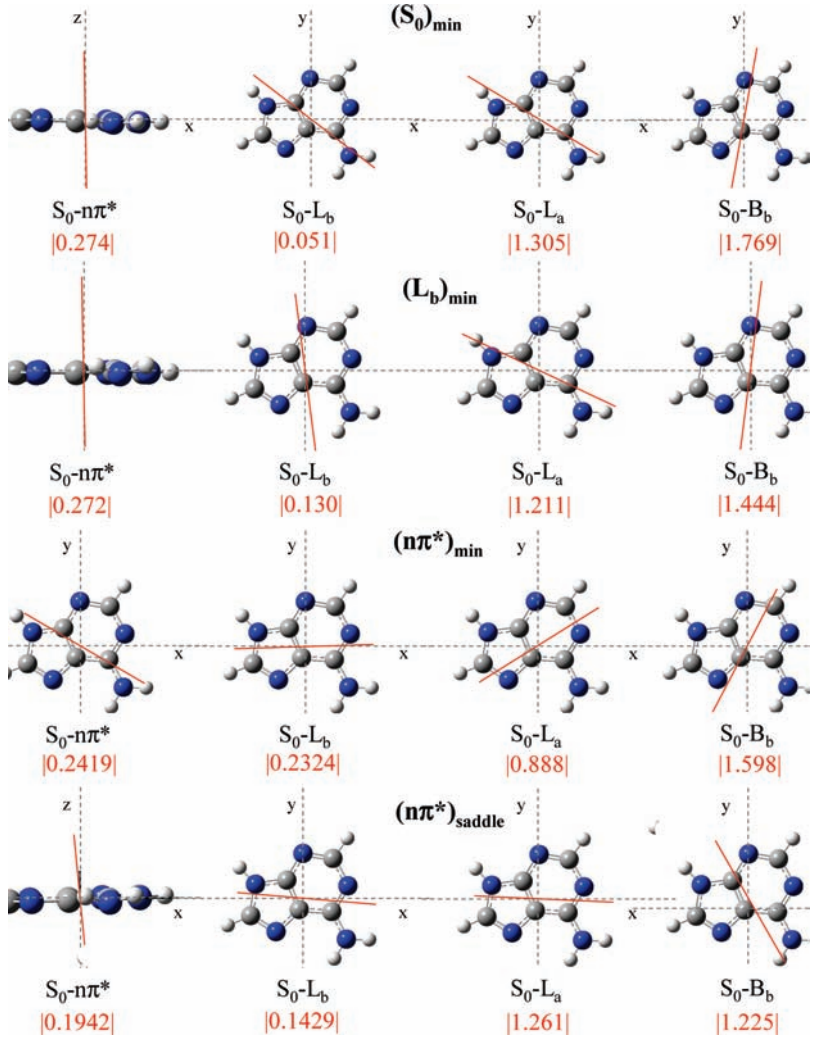

Figure 3. Graphical representation of the orientation of the $S_0 \leftrightarrow S_i$ TDMs computed (CASSCF level) at the $(S_0)_{min}$, $(^1L_b)_{min}$, $(^1n\pi^*)_{min}$, and $(^1n\pi^*)_{saddle}$ optimized structures. The number below each molecular picture is the computed magnitude (e bohr) of the TDM.

3.1.3. Vibrational Frequencies in the S_0, L_b, and $n\pi^*$ States. The knowledge of the vibrational frequencies of S_0 and of the lowest excited states, L_b and $n\pi^*$ states, are essential to discuss the vibronic structure of excitation spectra. To discuss the observed (mono) deuteration effects on the vibronic structure, we also determined the $(^1n\pi^*)_{min}$ frequencies of deuterated isotopomers. The complete list of vibrational frequencies computed for the $(S_0)_{min}$, $(^1L_b)_{min}$, $(^1n\pi^*)_{min}$, and $(^1n\pi^*)_{min}$ structures are collected in Tables S6 and S7 (see the Supporting Informations). The CASSCF/6-31+G** S_0 vibrational frequencies, uniformly scaled by 0.9, correlate well with the B3LYP/6-31G** results reported by Colarusso et al.[37] and with more recent CASSCF calculations[14] except for the 55 cm^{-1} frequency,[14] which is absent in our results. They are also in agreement with the IR frequencies obtained in matrix.[48]

Excited state frequencies collected in Tables S6−S11 (Supporting Informations) were also scaled by 0.9. To our knowledge the only term of comparison is represented by the recently computed CASSCF frequencies computed by Chin et al.[14] A number of differences are noted with respect to our results. In particular, these authors apparently found the same frequencies for the L_b and L_a states and an increase of frequencies going from S_0 to the L_b and to the L_a excited states, in contrast with our results.

A cursory examination of the normal coordinates indicates that Duschinsky mixing[30] is minor between modes of $(S_0)_{min}$ and $(^1L_b)_{min}$ and between $(S_0)_{min}$ and $(^1n\pi^*)_{saddle}$. In contrast, mode mixing between the normal coordinates of the $(^1n\pi^*)_{min}$ and S_0 and between the $(^1n\pi^*)_{min}$ and the $(^1n\pi^*)_{saddle}$ normal coordinates are more significant, not only in the range of frequencies correlating with the ring puckering coordinate (see also Table S8 in the Supporting Information).

3.2. Vibronic Structure Associated with the $S_0 \rightarrow L_b$ Transition. Because of the low symmetry of Ade, virtually all normal coordinates can either be FC active or steal intensity from strongly allowed transitions through the HT mechanism. Thus, both contributions have to be computed and compared for those modes relevant to the assignment of observed vibronic bands. We consider first the FC activities. The largest computed FC activities (γ_i parameters, see eq 8, proportional to the intensity of the 0−1 vibronic bands) are collected in Table 3. The S_0 and L_b equilibrium geometries are relatively similar and consequently most of the allowed $S_0 \leftrightarrow L_b$ intensity is expected to be concentrated on the vibronic origin 0−0 and at most on the 0−1 vibronic bands. The oscillator strength f_{0-1}^i of the 0−1 band for the ith vibrational mode and the f_{0-0} of the origin, can be obtained as $f_{0-1}^i = f(S_0 \rightarrow L_b)\exp(-\gamma_{tot})\gamma_i$, $f_{0-0} = f(S_0 \rightarrow L_b)\exp(-\gamma_{tot})$. Taking the average value of the CASPT2 computed $f(S_0-L_b)$ at the $(S_0)_{min}$ (3.2×10^{-4}) and $(^1L_b)_{min}$ (1.9×10^{-3}) geometries (see Table 1), we get $f(S_0 \leftrightarrow L_b) \approx 10^{-3}$. Since the $S_0 \leftrightarrow L_b$ transition moment is in-plane polarized and preferentially (2:1) along the short molecular axis (y), as shown in Figure 3, the oscillator strength is dominated (4:1) by the y component. According to the CASSCF computed geometries $\gamma_{tot} = 2.91$. However, in our experience,[49] geometry change upon excitation are often overestimated at CASSCF level of theory. Such overestimate is reflected in too large B_i values (see eq 6). Assuming that a more appropriate value is 80% of the computed B_i values, γ_{tot} reduces to 1.86, which appears a reasonable value. All the reported γ_i values (see Table 3) were scaled by the same factor 0.639 (1.86/2.91). The resulting computed oscillator strengths f_{0-1}^i are collected in the same table. Since all the γ_i values are <1, the 0−1 bands are the most intense in the FC progressions. Summarizing, the most active 0−1 bands are predicted to be at 478, 505, 915, 1020, and 1734 cm^{-1}. The intensities of all these bands are in-plane polarized with a 4:1 dominance of the y component.

TABLE 3: Franck−Condon Activities (I_i/I_{0-0}, i.e., γ_i Parameters) and Oscillator Strengths (f) for the 0−0 and 0−1 Bands of the Most Active Modes in the $S_0 \rightarrow L_b$ Transition

ν (cm^{-1})[a]	$\gamma_i = I_i/I_{0-0}$	$10^3 f_i^b$
0−0	1.000	0.156
399	0.097	0.015
412	0.044	0.007
478	0.223	0.035
505	0.185	0.029
554	0.077	0.012
647	0.108	0.017
816	0.057	0.009
887	0.084	0.014
915	0.397	0.062
1020	0.178	0.028
1350	0.031	0.005
1609	0.026	0.004
1734	0.346	0.054

[a] Excited state frequencies were uniformly scaled by 0.9. [b] The oscillator strength was evaluated assuming $\Delta E = 36\,105$ cm^{-1} from the experimental energy of the D band.[9]

TABLE 4: HT Computed Activities ($M_{S_0 0,L_b 1}^2$, Eq 3, Assuming All Other Vibrational Levels in Their Ground State) and Oscillator Strengths (f) for Selected Normal Modes of Ade in the L_b State

ν_i (cm^{-1})[a]	$10^5 M_{S_0 0,L_b 1}^2$ (e bohr)^2	$10^3 f$[c]
554	75	0.012
647	21	0.004
659	1	<0.001
816	8	0.001
887	505	0.084
915	15	0.003
990	1	<0.001

[a] Excited state frequencies were uniformly scaled by 0.9. [c] The oscillator strength was evaluated assuming $\Delta E = 36\,105$ cm^{-1} from the experimental energy of the D band[9] and it includes the FC factor as in eq 9 estimated to be $0.156(\exp(-\gamma_{tot}))$.

The HT induced TDMs collected in Table 4 were evaluated as described in section 2.2 for the normal modes whose associated frequencies fall in the region 500−1000 cm^{-1}. While most of the computed induced intensities are found to be rather weak, the oscillator strength associated with the 887 cm^{-1} frequency is 0.13×10^{-3}: this normal mode is expected to be one of the most intense vibronic bands associated with the $S_0 \rightarrow L_b$ transition. Interestingly, its intensity is in-plane polarized, and largely (2:1) along the short (y) axis (see Table S12, Supporting Informations), which suggests that it is borrowed mainly from the $S_0 \leftrightarrow B_b$ transition.

From the computed FC and HT activities it follows that the most intense bands of the $S_0 \leftrightarrow L_b$ excitation spectrum are predicted to be the origin band, the HT induced band at 887 cm^{-1} and the FC bands at 915, 1020, and 1734 cm^{-1}. It is worth noting that the FC activity of the 887 cm^{-1} frequency is very small, compared with its HT contribution, thus the HT−FC interference can be considered negligible for this false origin, which is expected to be the most intense among the $S_0 \leftrightarrow L_b$ vibronic bands. All the predicted bands are polarized predominantly along the short (y) axis. In view of the large computed intensity for the 0−0 band, we can conclude that the present

calculations confirm the so far accepted assignment of the D band in the R2PI spectra[9] to the origin of the $S_0 \leftrightarrow L_b$ transition.

3.3. Vibronic Structure Associated with the $S_0 \rightarrow n\pi^*$ Transition. The vibronic bands of the $S_0 \rightarrow {}^1n\pi^*$ transition arise from excitations to the vibronic levels of the anharmonic puckering mode or to those of harmonic modes, or both. We consider the two sets of modes as separable. First we discuss the transitions to vibronic levels of the anharmonic puckering potential and separately estimate the contributions from harmonic modes. Finally we take into account their interrelation. Accordingly, the expression of the oscillator strength f for either FC or HT induced activities is recast in a formulation underscoring the separation between the anharmonic puckering mode and harmonic modes. It is worth noting the particular role played by the puckering mode in the spectroscopic and photophysical properties of Adenine and of other DNA bases. In Ade it contributes substantially to the vibronic structure of the $S_0 \rightarrow {}^1n\pi^*$ transition, as shown presently, and plays an essential role in the ultrafast deactivation of the ^1L_a excited state.[42,43]

The oscillator strength associated with the $0-1$ transition of the ith FC active harmonic mode, and the $0-m$ transition in the anharmonic modes (with all the remaining harmonic modes in their ground vibrational level), is

$$\begin{aligned} f^i_{0-1(\text{harmonic});0-m(\text{anharm})} &= \frac{2}{3}h\nu\langle\chi_0^{S_0}|\mu_{S_0,n\pi^*}|\chi_m^{n\pi^*}\rangle^2 \exp(-\gamma_{\text{tot(harmonic)}})\gamma_{i,\text{harmonic}} \\ &= \frac{2}{3}h\nu(M_{S_0 0,n\pi^* m})^2_{\text{anharm}} \exp(-\gamma_{\text{tot(harmonic)}})\gamma_i \end{aligned} \quad (12)$$

where the vibronic integral $\langle\chi_0^{S_0}|\mu_{S_0},n\pi^*|\chi_m^{n\pi^*}\rangle^2$ is computed numerically according to eq 13, similarly

$$f^i_{0-0(\text{harmonic});0-m(\text{anharm})} = \frac{2}{3}h\nu(M_{S_0 0,n\pi^* m})^2_{\text{anharm}} \exp(-\gamma_{\text{tot(harmonic)}}) \quad (13)$$

For the $0-1$ HT induced activity of the ith harmonic mode, and the $0-m$ transition in the anharmonic modes (with all the remaining harmonic modes in their ground vibrational level), we employ the following reformulation of eq 4

$$f^i_{0-1(\text{HT,harmonic});0-m(\text{anharm})} = \frac{2}{3}h\nu_{K0_i,J1_i}M^2_{K0_i,J1_i}\exp(-\gamma_{\text{tot(harmonic)}})\langle 0|m\rangle^2_{\text{anharm}} \quad (14)$$

where the overlap integral $\langle\chi_0^{S_0}|\chi_m^{n\pi^*}\rangle = \langle 0|m\rangle_{\text{anharm}}$ is computed numerically according to eq 12.

3.3.1. Vibronic Structure Determined by the Anharmonic Puckering Coordinate. The contribution of the anharmonic potential for the puckering mode is very important because it can generate an extended vibronic structure. In particular it can explain the anomalous intensity ratio (ca. 10:1) between the observed C and A bands,[9] where the latter band has been so far assigned to the origin of the $S_0 \rightarrow n\pi^*$ transition. As discussed in section 2, in the 2D flexible model, the puckering mode is coupled with the C_2-H out-of-plane bending mode. Keeping in mind the form of the $^1n\pi^*$ two-dimensional potential given in eq 10, we considered a selection of a, b parameters such to produce energy barriers E_b and minima for puckering angles ϕ_0 ranging from $E_b = 1125$ cm^{-1}, $\phi_0 = 25°$ to $E_b = 3600$ cm^{-1}, $\phi_0 = 36°$.

TABLE 5: Proposed Assignment of the Observed[9] Bands A and C to Vibronic Transitions in the Puckering Coordinate (Representative Results from Several Combinations of Potential Energy Parameters Employed in the 2D Flexible Model[34])

E_b (cm^{-1})	ϕ_0 (deg)	E (cm^{-1})[a]	$10^3(M^z_{S_0,n\pi^*})^2$[b] (e bohr)^2	$(S_{S_0,n\pi^*})^2$	$10^3 f$[c]	E (C−A)[e]	I (C/A)[f]
2000	31.6	1195[a]	0.503	0.11	0.054		
2000	33	1148[a]	0.311	0.07	0.034		
2100	30	1277[a]	0.594	0.13	0.064		
2100	32	1218[a]	0.382	0.08	0.041		
2220	33	1217[a]	0.212	0.05	0.023		
2000	31.6	1649[d]	2.441	0.53	0.267	454	4.8
2000	33	1593[d]	1.868	0.41	0.205	445	5.9
2100	30	1737[d]	2.437	0.53	0.267	460	4.2
2100	32	1698[d]	2.214	0.48	0.242	480	5.9
2220	33	1709[d]	1.413	0.31	0.155	492	6.2

[a] Predicted energy of band A. This computed energy along with the computed vibronic transition moments and overlaps, correspond to the $0 \rightarrow 6$ vibronic transition in the puckering coordinate. [b] Note that $(M_{S_0,n\pi^*})$ and $(M_{S_0,n\pi^*})^2$ are negligible for all the transitions. [c] These computed f do not include the contributions from harmonic modes. [d] Predicted energy of band C. This computed energy along with the computed vibronic transition moments and overlaps, correspond to the $0 \rightarrow 12$ vibronic transition in the puckering coordinate. [e] Computed energy difference between the vibronic transitions assigned to band C and A. [f] Computed intensity ratio between the vibronic transitions assigned to band C and A.

Overlap integrals $S_{S_0,n\pi^*}$ and vibronic transition moments $M^w_{S_0,n\pi^*}$ were computed according to eq 12 employing, for the latter, the functional dependence on ϕ of the electronic TDMs $\mu^x_{S_0,n\pi^*}$, $\mu^y_{S_0,n\pi^*}$ and $\mu^z_{S_0,n\pi^*}$, defined in eq 11.

A general trend shown by the simulations is that negligible intensity is predicted for the $0-0$ transition. As a result, the so far accepted assignment of the A band to the origin of the $S_0 \rightarrow n\pi^*$ transition must be reconsidered. The emerging indication from the several simulations carried out is that band A should be assigned to a transition to a relatively large quantum number in the puckering coordinate. As a consequence, the origin of the $S_0 \rightarrow n\pi^*$ transition is expected to be located about $1000-1200$ cm^{-1} below the observed A band and because of its predicted negligible intensity is unlikely to be observed. A selection of results from model calculations giving satisfactory assignments of bands A and C and realistic values for the E(C) $-$ E(A) energies along with intensity ratios f(C)/f(A) is collected in Table 5. These results suggest the more appropriate values for E_b and ϕ_0. Larger energy barriers would lead to significant intensities only for transitions to very high vibronic levels of the $n\pi^*$ state.

According to calculations, all the intensities associated to vibronic transitions up to the 19th vibrational level of the puckering coordinate in the $n\pi^*$ state are polarized along z. The ratio between the intensities of the transitions assigned to bands A and C is found to vary from 1:4.2 to 1:6.2, and the E(C) $-$ E(A) energy difference from 445 to 492 cm^{-1}. The corresponding experimental data for bands A and C are intensity ratio 1:10 and $\Delta E = 565$ cm^{-1}.[6]

The puckering (out-of-plane) vibration in its even quantum numbers v (in the $n\pi^*$ state) behaves as a FC active mode, and correspondingly, these transitions are polarized along the z axis as an $S_0 \rightarrow n\pi^*$ transition should be. However, this vibration should also act as an inducing mode coupling the $n\pi^*$ with a $\pi\pi^*$ state (L_a or B_b). Thus, transitions to the odd v vibrational levels should be associated with nonzero $(M^x_{S_0,n\pi^*})^2$ and $(M^x_{S_0,n\pi^*})^2$ integrals. Surprisingly, for odd v up to 19 these integrals are

TABLE 6: FC Activities (I_i/I_{0-0}, i.e., γ_i Parameters) and Oscillator Strengths (f) for the 0−0 and 0−1 Bands of the Most Active Modes in the $S_0 \rightarrow n\pi^*$ Transition

ν_i (cm^{-1})[a]	$\gamma_i = I_i/I_{0-0}$ $\gamma_{tot} = 2.125$	$\gamma_i = I_i/I_{0-0}$ $\gamma_{tot} = 3.06$
0−0	1.00	1.00
382	0.142	0.21
475	0.175	0.25
676	0.215	0.31
690	0.130	0.19
899	0.200	0.29
935	0.405	0.58
943	0.085	0.12
1023	0.335	0.48
1087	0.072	0.10
1174	0.122	0.18
1352	0.050	0.07
1422	0.180	0.26

[a] Excited state frequencies were uniformly scaled by 0.9.

TABLE 7: HT Computed Activities ($M^2_{S_0 0,L_b 1}$, see eq 3) and Oscillator Strengths (f) for Selected Normal Modes of Ade in the $n\pi^*$ State

ν_i (cm^{-1})[a]	$10^5 M^2_{S_0 0,np^*1}$ (e bohr)^2	$10^3 f$[b,c]	$10^3 f$[b,d]
199	66.4	0.009	0.004
306	431.4	0.057	0.022
621	158.2	0.021	0.008
676	169.7	0.022	0.009
698	107.3	0.014	0.006

[a] Excited state frequencies were uniformly scaled by 0.9. [b] The oscillator strength was evaluated assuming $\Delta E = 36\,248$ cm^{-1}, from the experimental value of the E band[9] and including the FC factor due to harmonic modes, estimated as $\exp(-\gamma_{tot})$. [c] The FC factor was estimated assuming $\gamma_{tot} = 2.125$. [d] The FC factor was estimated assuming $\gamma_{tot} = 3.06$.

computed to be negligible with all the E_b, ϕ_0 parameters considered, indicating that the intensity borrowing activity of the anharmonic mode is negligible.

3.3.2. FC and HT Activities Associated with Harmonic Modes. While the intensities associated with the vibronic levels of the anharmonic puckering mode were discussed on the basis of an anharmonic model, the contributions from the other modes can be determined assuming the harmonic approximations as discussed for the $S_0 \rightarrow L_b$ transition. First we discuss the computed FC intensities. The computed γ parameters providing estimates for the 0−1 bands intensities are collected in Table 6. According to CASSCF optimized geometries $\gamma_{tot} = 8.5$. This is a rather large value, which derives most likely from an overestimate of the value of B_i parameters. Assuming that the correct B_i are 50% (or 60%) of the computed values, the γ_{tot} reduces to 2.125 (or 3.06), which appear reasonable values. The two sets of γ_i values reported in Table 6 are reduced correspondingly. From the computed γ_i the most intense FC active bands are predicted to be at 935 and 1023 cm^{-1}, but an appreciable activity is associated with the modes whose frequencies are 382, 475, 676, 899, and 1422 cm^{-1}.

The HT induced TDMs collected in Table 7 were evaluated as described in section 2.2 for the normal modes whose associated frequencies fall in the region 0−700 cm^{-1}. The most active modes are those corresponding to frequencies 306 (out of plane), 621, 676, and 698 cm^{-1}.

3.4. Comparison between Computed Vibronic Activities and the Observed R2PI Spectra. The jet cooled R2PI spectra,[6,7,9] show a number of discrete bands below the onset of the diffuse spectrum associated with the L_a state. The lowest, named A band, is observed at 35 497 cm^{-1}, 4.40 eV, an energy very similar to the computed $^1n\pi^*$ energy minimum (4.44 eV). It is very weak and it has been assigned, generally, to the 0−0 band of the $S_0 \leftrightarrow n\pi^*$ transition. The next C, D, and E bands, which are located at 36 062, 36 105, and 36 248 cm^{-1}, respectively, are ca. 10, 34, and 10 times more intense than band A. The C and E bands in the jet cooled R2PI spectra[9] exhibit the same deuteration effects while band D shows a different structure. Furthermore, the dispersed fluorescence spectra obtained by exciting the C and D bands show different vibrational structures.[10] These observations indicate that bands C and E belong to the same electronic excitation, which is different from that responsible for band D. The generally accepted assignment[6] is that bands C and E are[9,10] vibronic bands of the $^1n\pi^*$ state based on 565 and 751 cm^{-1} frequency vibrations. The D band, observed at 36 105 cm^{-1}, is assigned to the origin of the $S_0 \rightarrow L_b$ transition.

As discussed above, the R2PI spectrum shows four major bands (A, C, D, and E) and a number of additional vibronic details, generally attributed to two electronic transitions: the $S_0 \rightarrow n\pi^*$ and the $S_0 \rightarrow L_b$. We can now combine all the information presented in the previous subsections and provide an assignment of the observed spectrum on the basis of the computed $S_0 \rightarrow n\pi^*$ and $S_0 \rightarrow L_b$ vibronic activities.

While vibronic bands of the $S_0 \leftrightarrow L_b$ transition are generated by harmonic oscillators, the vibronic bands associated with the $S_0 \rightarrow n\pi^*$ spectrum result from transitions to vibronic levels of the harmonic modes, of the anharmonic modes, or both. Thus, the oscillator strengths must be evaluated according to eqs 13−14. The resulting computed oscillator strengths associated with the $S_0 \rightarrow n\pi^*$ and the $S_0 \rightarrow L_b$ transitions, as emerging from the modeling, are collected in Table 8. Although the five selected potentials for the anharmonic coordinate listed in Table 5 provide similar indications, in the following discussion (and in Table 8) we selected the results obtained from $E_b = 2000$ cm^{-1} and $\phi_0 = 31.6°$ and used the computed vibronic TDMs and overlap integrals resulting from this set of simulations.

The data reported in Table 8 support, in part, the generally accepted interpretation of the R2PI spectrum, but they also provide novel assignments. First, the generally accepted assignment of band A as the origin of the $S_0 \rightarrow n\pi^*$ transition must be reconsidered on the basis of our modeling. Fundamental was, in this sense, the identification (via CASSCF calculations) of a remarkably anharmonic potential along the puckering coordinate of the 6-atom ring of Ade. Modeling of vibronic intensities in the framework of the 2D flexible model[34] definitely rules out the attribution of band A to the 0−0 transition, since its intensity is predicted to be negligible in all the simulations considered. In contrast, as indicated in Table 8, band A is assigned to a vibronic transition to the sixth level of the puckering coordinate in the $n\pi^*$ state. Because of the markedly anharmonic potential, the transition to an even higher vibronic level (the 12th) of the $n\pi^*$ state is predicted ca. 5−6 times more intense than the transition assigned to band A. Thus, we readily assign this transition to band C also because of its energy matching closely the observed value.

Both bands A and C act as false origins on which harmonic modes can build their vibrational structure. On this basis, we can assign band E and a number of previously unassigned bands to transitions involving combinations of the anharmonic level (the 6th or the 12th) and of a harmonic fundamental (see Table 8). In particular, band E, whose intensity is predicted to be similar to that of band C (in nice agreement with observations) originates from the HT induced activity of a mode which steals

TABLE 8: Overall Vibronic Activity Computed for the $S_0 \rightarrow n\pi^*$ and $S_0 \rightarrow L_b$ Transitions and Proposed Assignment of the R2PI Observed Bands[6,9] [a]

vibronic levels involved	computed energy[b] ν (cm^{-1})	$10^6 f_i$	$10^6 f_i$	relative intensity observed	assignment to observed bands (cm^{-1})
Vibronic Bands Deriving from the $S_0 \rightarrow n\pi^*$ Transition and Built over Band A					
$(0-0)_{har}$, $(0-6)_{an}$	1195	6.4[c]	2.5[d]	0.02	35 497[g] (band A)
$(0-1)_{har}$, HT, $(0-6)_{an}$	1195 + 306	6.3[c]	2.4[d]		under band B
$(0-1)_{har}$, FC, $(0-6)_{an}$	1195 + 382	0.9[c]	0.5[d]		
$(0-1)_{har}$, FC, $(0-6)_{an}$	1195 + 475	1.1[c]	0.6[d]		
$(0-1)_{har}$, FC, $(0-6)_{an}$	1195 + 676	1.4[c]	0.8[d]	0.1	36 167[g]
Vibronic Bands Deriving from the $S_0 \rightarrow n\pi^*$ Transition and Built over Band C					
$(0-0)_{har}$, $(0-12)_{an}$	1649	31.9[e]	12.5[f]	0.25	36 062[g] band C)
$(0-1)_{har}$, HT, $(0-12)_{an}$	1649 + 306	30.2[e]	11.7[f]	0.4	36 248[g] (band E)
$(0-1)_{har}$, FC, $(0-12)_{an}$	1649 + 382	4.5[e]	2.6[f]	0.05	36 415[g]
$(0-1)_{har}$, FC, $(0-12)_{an}$	1649 + 475	5.6[e]	3.1[f]	0.27	36 519[g]
$(0-1)_{har}$, HT, $(0-12)_{an}$	1649 + 621	11.1[e]	4.2[f]		36 728[h]
$(0-1)_{har}$, HT, $(0-12)_{an}$	1649 + 676	11.7[e]	4.8[f]		36 785[h]
$(0-1)_{har}$, FC, $(0-12)_{an}$	1649 + 676	6.9[e]	3.9[f]		
Vibronic Activity Deriving from the $S_0 \rightarrow L_b$ Transition					
0−0	0	156		1	36 105[g] (band D)
0−1 FC	399	15			36 498[g]
0−1 FC	412	7		0.27	36 519[g]
0−1 FC	478	35		0.18	36 600[h]
0−1 FC	505	29		0.18	36 600[h]
0−1 HT	554	12		0.05	36 632[h]
0−1 FC	554	12			

[a] For the $S_0 \rightarrow n\pi^*$ transition we collected the vibronic activity (due to harmonic modes) built over the two most active transitions computed upon excitation of the puckering coordinate, and assigned to observed bands A and C, respectively. The set of 2D potential results chosen corresponds to $E_b = 2000$ cm^{-1}, $\phi_0 = 31.6°$ (see Table 5). [b] Energy above the 0−0 transition. [c] f computed according to eqs 13−14 using the data collected in the previous tables, more specifically $(S_{S_0,n\pi^*})_{anharm}^2 = 0.11$ and $(\gamma_{tot})_{harmonic} = 2.125$ for the $S_0 \rightarrow n\pi^*$ transition. [d] f computed according to eqs 13−14 using the data collected in the previous tables, more specifically $(S_{S_0,n\pi^*})_{anharm}^2 = 0.11$ and $(\gamma_{tot})_{harmonic} = 3.06$ for the $S_0 \rightarrow n\pi^*$ transition. [e] f computed according to eqs 13−14 using the data collected in the previous tables, more specifically $(S_{S_0,n\pi^*})_{anharm}^2 = 0.53$ and $(\gamma_{tot})_{harmonic} = 2.125$ for the $S_0 \rightarrow n\pi^*$ transition. [f] f computed according to eqs 13−14 using the data collected in the previous tables, more specifically $(S_{S_0,n\pi^*})_{anharm}^2 = 0.53$ and $(\gamma_{tot})_{harmonic} = 3.06$ for the $S_0 \rightarrow n\pi^*$ transition. [g] From ref 9. [h] From ref 6.

intensity from $\pi\pi^*$ transitions. Thus, this band is expected to have an in-plane polarization, as it has been shown by the observations of rotational band contours.[13]

Several observed bands of lower intensity can be tentatively assigned to computed vibronic levels associated with significant FC or HT activity. Indeed, the computed vibrational structure based on band C can almost entirely find its counterpart in the observed bands (see Table 8). Among these are the bands at 36 728 and 36 785 cm^{-1} taken from the top end of the R2PI spectrum of ref 6. The weak band observed at 36 167 cm^{-1} is the only band that can be assigned to the structure based on A.

The observed band intensities appear to decrease with increasing energy and they are eventually smeared out in the incipient L_a intense band. In this respect, it must be noted that band intensities in the R2PI spectra may decrease with the increasing energy also because the nonradiative decay rate increases with the energy. This may account for partial discrepancies in predicted versus observed intensities.

To complete the discussion, we also include in Table 8 the predicted oscillator strength of the D band, which is assigned as the origin of the $S_0 \rightarrow L_b$ transition and of its associated vibronic structure. A number of features observed in the R2PI spectrum are tentatively assigned to vibronic bands of the $S_0 \rightarrow L_b$ transition. In passing, we note that the predicted relative intensities of bands A, C, D, and E, belonging to two different electronic transitions, are well reproduced by the simulations.

The rotational band profile analysis recently performed[13] provides further information on the bands C, D, and E. In particular, the polarization of their transition moments can be extracted. The components of transition intensities of the C, D, and E bands are given with respect to the *a*, *b*, *c* inertial axes, which correspond essentially to the *x* (short), *y* (long) and *z* (out-of-plane) axes. The experimentally determined[13] components' intensities are in the ratios: 0.09*a*, 0.17*b*, 0.74*c* for band C, 0.18*a*, 0.63*b*, 0.19*c* for band D, 0.26*a*, 0.53*b*, 0.21*c* for band E. These polarization data are in agreement with our computed results. In fact, band C and D correspond to the $S_0 \rightarrow n\pi^*$ (out of plane, or *c*(z) polarized) and $S_0 \rightarrow L_b$ (in plane polarized) transitions, respectively. It is to be noted that $S_0 \rightarrow L_b$ is polarized along the *b* (short in-plane) axis, which is roughly the same as the polarization of the $S_0 \rightarrow B_b$ transition. The intensity of band E, which is borrowed from $S_0 \rightarrow \pi\pi^*$ transitions, is observed to be polarized predominantly along the *b* axis. Our computed HT induced TDMs (see Table S13 in the Supporting Information) indicate equivalent contributions from the two in-plane polarizations. Since the *x*(*a*) or *y*(*b*) polarization of the C and D bands may indicate the dominant coupling between the borrowing ^1L_b and $^1n\pi^*$ states and the $^1\pi\pi^*$ (L_a and B_b) lending states, this information can be useful to clarify not only the origin of the borrowed intensity but also the mechanism of deactivation of the ^1L_b and $^1n\pi^*$ states. Specifically, our calculations and the polarization measures seem to indicate that the coupling between the $^1L_b/^1n\pi^*$, and the ^1L_a state is not particularly strong.

To the best of our knowledge, the vibrational structure of the absorption spectrum of Ade has been investigated only by one group.[14] This analysis, which did not consider the anharmonicity of the puckering coordinate, arrived at different conclusions from ours. The intensities of the A and C bands, which are based on the $^1n\pi^*$ state, were attributed to the Franck−Condon mechanism and to the $^1n\pi^*-^1\pi\pi^*$ vibronic coupling, respectively. The D and E bands were considered as

vibronic bands of interacting $^1\pi\pi^*$ states. These assignments differ from ours and, more importantly, are in contrast with the measured transition moment polarization reported in ref 13.

4. Conclusions

We have presented a computational study encompassing high-level quantum-chemical calculations of the ground and low-lying excited states of 9*H*-adenine and modeling of vibronic activities, associated with the $S_0 \rightarrow L_b$ and $S_0 \rightarrow n\pi^*$ transitions, which included harmonic and anharmonic contributions. The picture emerging from the presented modeling of vibronic activities supports, in general, the accepted interpretation but provides new relevant information on the active vibrational modes in the two electronic transitions, and new detailed assignments as well as indications on dominant couplings between low-lying electronic states.

The study underscores, for the first time, the role of the double-minimum potential associated with the puckering of the 6-atom ring in determining vibronic activities. Band A and band C in the R2PI spectra are assigned to transitions to vibronic levels of the puckering coordinate or combinations of the puckering coordinate and other harmonic modes, as is the case for band E, which is vibronically induced via an out of plane mode.

Band A is reassigned as the transition to the lowest vibronic level of the $^1n\pi^*$ *that is observed*, but not necessarily to the true lowest vibronic level. In fact, the vibronic transition is computed ca. 1000 cm^{-1} above the 0−0, which, according to our analysis, has escaped detection so far.

Band C is shown to be due to a transition to an even higher vibronic level of the anharmonic mode belonging to the $^1n\pi^*$ state. It is the very anharmonicity of the potential associated with this coordinate that makes this transition about 10 times larger than band A. Both bands A and C act as false origins on which harmonic modes can build their vibrational structure.

This latter observation explains the appearance of band E, also belonging to the $^1n\pi^*$ state, which is a vibronic transition to a combination of harmonic and anharmonic vibrational levels. More specifically, to the fundamental of a low-frequency out-of-plane mode stealing intensity from $\pi\pi^*$ states and to the same vibrational level of the anharmonic mode associated with band C. Finally, this study confirms the previously proposed assignment of band D to the origin of the $S_0 \rightarrow L_b$ transition. Interestingly, the predicted relative intensities of the four major bands of the R2PI spectrum agree with the observed counterparts and are almost unsensitive to the parameters chosen for the 2D flexible model in a relatively large range.

From the computed HT induced TDMs it is concluded that coupling between the L_b and the B_b states dominates, while the $^1n\pi^*$ state is coupled with both the L_a and B_b states, a result that can be useful to understand the mechanism of deactivation of the two low-lying excited states.

Acknowledgment. This work was supported by funds from MIUR: grant ex 60% and PRIN Project 2007 NZLYE5_001 "Energy and charge transfer: from collisions to dissipative processes".

Supporting Information Available: Four figures including the 2D potential employed in the flexible anharmonic model, additional ground state geometries, a graphical representation of the normal coordinates of the ground state and of those computed at the $(^1n\pi^*)_{saddle}$ structure. Thirteen tables including the parameters employed to fit the 2D flexible model, CASSCF and CASPT2 absolute energies, Cartesian components of the TDMs computed at several geometries, full list of vibrational frequencies in the ground and excited states, along with deuteration effects, Cartesian components of HT induced TDMs, Cartesian coordinates of the structures discussed in the text. This material is available free of charge via the Internet at http://pubs.acs.org.

References and Notes

(1) Callis, P. R. *Annu. Rev. Phys. Chem.* **1983**, *34*, 329–357.
(2) Daniels, M. *Photochemistry and Photobiology of Nucleic Acids*; Academic Press: New York, 1976; Vol. 1.
(3) Crespo-Hernandez, C. E.; Cohen, B.; Hare, P. M.; Kohler, B. *Chem. Rev.* **2004**, *104*, 1977–2020.
(4) Clark, L. B.; Peschel, G. G.; Tinoco, I. *J. Am. Chem. Soc.* **1965**, *87*, 11–15.
(5) Middleton, C. T.; de La Harpe, K.; Su, C.; Law, Y. K.; Crespo-Hernández, C. E.; Kohler, B. Annu. Rev. Phys. Chem. 2009, *60*.
(6) Kim, N. J.; Jeong, G.; Kim, Y. S.; Sung, J.; Kim, S. K.; Park, Y. D. *J. Chem. Phys.* **2000**, *113*, 10051.
(7) Lührs, D. C.; Viallon, J.; Fischer, I. *Phys. Chem. Chem. Phys.* **2001**, *3*, 1827–1831.
(8) Plützer, C.; Nir, E.; de Vries, M. S.; Kleinermanns, K. *Phys. Chem. Chem. Phys.* **2001**, *3*, 5466.
(9) Plützer, C.; Kleinermanns, K. *Phys. Chem. Chem. Phys.* **2002**, *4*, 4877.
(10) Kim, N. J.; Kang, H.; Park, Y. D.; Kim, S. K. *Phys. Chem. Chem. Phys.* **2004**, *6*, 2802.
(11) Nir, E.; Pltzer, C.; Kleinermanns, K.; de Vries, M. *Eur. Phys. J. D* **2002**, *20*, 317.
(12) Hünig, I.; Pltzer, C.; Seefeld, K. A.; Lwenich, D.; Nispel, M.; Kleinermanns, K. *Chemphyschem* **2004**, *5*, 1427.
(13) Lee, Y.; Schmitt, M.; Kleinermanns, K.; Kim, B. *J. Phys. Chem. A* **2006**, *110*, 11819–11823.
(14) Chin, C.-H.; Mebel, A. M.; Kim, G.-S.; Baek, K. Y.; Hayashi, M.; Liang, K. K.; Lin, S. H. *Chem. Phys. Lett.* **2007**, *445*, 361–369.
(15) Roos, B. O. In *Advances in Chemical Physics: Ab Initio Methods in Quantum Chemistry*; Lawley, K. P., Ed.; (John Wiley & Sons Ltd: Chichester, 1987; Vol. 69, p 399.
(16) Malmqvist, P.-A.; Roos, B. O. *Chem. Phys. Lett.* **1989**, *155*, 189–194.
(17) Försberg, N.; Malmqvist, P.-Å *Chem. Phys. Lett.* **1997**, *274*, 196–204.
(18) Frisch, M. J. Trucks G. W. Schlegel, H. B. Scuseria, G. E. Robb, M. A. Cheeseman, J. R. Montgomery, J. A., Jr., Vreven, T. Kudin, K. N. Burant, J. C. Millam, J. M. Iyengar, S. S. Tomasi, J. Barone, V. Mennucci, B. Cossi, M., Scalmani, G. Rega, N. Petersson, G. A. Nakatsuji, H. Hada, M. Ehara, M. Toyota, K., Fukuda, R. Hasegawa, J. Ishida, M. Nakajima, T. Honda, Y. Kitao, O. Nakai, H. Klene, M., Li, X., Knox, J. E. Hratchian, H. P., Cross, J. B. Adamo, C. Jaramillo, J. Gomperts, R. Stratmann, R. E. Yazyev, O., Austin, A. J. Cammi, R. Pomelli, C. Ochterski, J. W. Ayala, P. Y. Morokuma, K. Voth, G. A. Salvador, P. Dannenberg, J. J., Zakrzewski, V. G. Dapprich, S. Daniels, A. D. Strain, M. C. Farkas, O. Malick, D. K., Rabuck, A. D. Raghavachari, K., Foresman, J. B. Ortiz, J. V. Cui, Q. Baboul, A. G. Clifford, S. Cioslowski, J. Stefanov, B. B. Liu, G. Liashenko, A. Piskorz, P. Komaromi, I. Martin, R. L. Fox, D. J. Keith, T. Al-Laham, M. A. Peng, C. Y. Nanayakkara, A. Challacombe, M. Gill, P. M. W. Johnson, B. Chen, W. Wong, M. W. Gonzalez, C. Pople, J. A. *Gaussian 03, Revision C.02*, Gaussian, Inc., Gaussian, Inc.: Wallingford, CT, 2004.
(19) *MOLCAS version 6.2*, Krogh, J. W. et al. (2003) Lund, Lund University.
(20) Negri, F.; Orlandi, G. In *Computational Photochemistry*; Olivucci, M., Ed.; Elsevier: 2005; Vol. 16, p 129−169.
(21) Di Donato, E.; Vanzo, D.; Semeraro, M.; Credi, A.; Negri, F. *J. Phys. Chem. A* **2009**, *113*, 6504–6510.
(22) Santoro, F.; Lami, A.; Improta, R.; Bloino, J.; Barone, V. *J. Chem. Phys.* **2008**, *128*, 224311.
(23) Barone, V.; Bloino, J.; Biczysko, M.; Santoro, F. *J. Chem. Theory Comput.* **2009**, *5*, 540–554.
(24) Jankowiak, H. C.; Stuber, J. L.; Berger, R. *J. Chem. Phys.* **2007**, *127*, 234101.
(25) Santoro, F.; Improta, R.; Lami, A.; Bloino, J.; Barone, V. *J. Chem. Phys.* **2007**, *126*, 084509.
(26) Santoro, F.; Lami, A.; Improta, R.; Barone, V. *J. Chem. Phys.* **2007**, *126*, 184102.
(27) Dierksen, M.; Grimme, S. *J. Chem. Phys.* **2005**, *122*, 244101.
(28) Borrelli, R.; Peluso, A. *J. Chem. Phys.* **2003**, *119*, 8437–8448.

(29) Keszthelyi, T.; Balakrishnan, G.; Wilbrandt, R.; Yee, W. A.; Negri, F. *J. Phys. Chem. A* **2000**, *104*, 9121–9129.
(30) Duschinsky, F. *Acta Physicochim. URSS* **1937**, *7*, 551.
(31) Zgierski, M. Z. *Chem. Phys.* **1986**, *108*, 61–68.
(32) Dierksen, M.; Grimme, S. *J. Chem. Phys.* **2004**, *120*, 3544–3554.
(33) Grimme, S. In *Reviews in Computational Chemistry*, Vol 20; WILEY-VCH, inc: New York, 2004, p 153−218.
(34) Meyer, R. *J. Mol. Spectrosc.* **1979**, *76*, 266.
(35) Emanuele, E.; Orlandi, G. *J. Phys. Chem. A* **2005**, *109*, 6471–6482.
(36) Orlandi, G.; Gagliardi, L.; Melandri, S.; Caminati, W. *J. Mol. Struct.* **2002**, *612*, 383–391.
(37) Colarusso, P.; Zhang, K. Q.; Guo, B. J.; Bernath, P. F. *Chem. Phys. Lett.* **1997**, *269*, 39–48.
(38) Choi, M. Y.; Dong, F.; Han, S. W.; Miller, R. E. *J. Phys. Chem. A* **2008**, *112*, 7185–7190.
(39) Brown, R. D.; Godfrey, P. D.; McNaughton, D.; Pierlot, A. P. *Chem. Phys. Lett.* **1989**, *156*, 61–63.
(40) McMullan, R. K.; Benci, P.; Craven, B. M. *Acta Cryst. B* **1980**, *36*, 1424.
(41) Yamazaki, S.; Kato, S. *J. Am. Chem. Soc.* **2007**, *129*, 2901–2909.
(42) Merchan, M.; Serrano-Andres, L. *J. Am. Chem. Soc.* **2003**, *125*, 8108–8109.
(43) Blancafort, L. *J. Am. Chem. Soc.* **2006**, *128*, 210–219.
(44) Marian, C. M. *J. Chem. Phys.* **2005**, *122*, 104314.
(45) Mennucci, B.; Toniolo, A.; Tomasi, J. *J. Phys. Chem. A* **2001**, *105*, 4749–4757.
(46) Perun, S.; Sobolewski, A. L.; Domcke, W. *J. Am. Chem. Soc.* **2005**, *127*, 6257.
(47) Chen, H.; Li, S. *J. Phys. Chem. A* **2005**, *109*, 8443.
(48) Nowak, M. J.; Lapinski, J. S.; Kwiatkowski, J. S.; Leszczynski, J. *J. Phys. Chem.* **1996**, *100*, 3527.
(49) Negri, F.; Zgierski, M. Z. *J. Chem. Phys.* **1993**, *99*, 4318–4326.

JP905795N